This manuscript is a work of the U.S. Government and is not subject to copyright.
It will be published in *Metrology, Inspection, and Process Control for Microlithography XX*,
C.N. Archie, Editor, Proc. SPIE **6152** (2006).

Scatterfield microscopy using back focal plane imaging with an engineered illumination field

Heather J. Patrick,*[a] Ravikiran Attota,[b] Bryan M. Barnes,[b] Thomas A. Germer,[a]
Michael T. Stocker,[b] Richard M. Silver,[b] and Michael R. Bishop[c]

[a]*Optical Technology Division, National Institute of Standards and Technology, Gaithersburg, MD 20899*
[b]*Precision Engineering Division, National Institute of Standards and Technology, Gaithersburg, MD 20899*
[c]*International SEMATECH, Austin, TX 78741*

ABSTRACT

We have implemented back focal plane (conoscopic) imaging in an optical microscope that has also been modified to allow selection of the illumination angles and polarization at the sample, and collected back focal plane images of silicon on silicon grating scatterometry targets with varying line widths. Using a slit illumination mask, the zero-order diffraction versus angle for –60° to +60° incident angles at a given polarization was obtained from a single image. By using reference images taken on a flat silicon background, we correct the raw target images for illumination source inhomogeneities and polarization-dependent transmission of the optics, and convert them to reflectance versus angle data for s- and p-polarizations, similar to that obtained from angle-resolved grating scatterometry. As with conventional scatterometry, the target lines need not be resolved for the reflectance signature to show sensitivity to small changes in the grating parameters. For a series of 300 nm pitch targets with line widths from 150 nm to 157 nm, we demonstrate nanometer-level sensitivity to line width with good repeatability, using 546 nm illumination. Additionally, we demonstrate a technique for separating the zero order from higher order diffraction on targets with multiple diffraction orders, allowing collection of both zero and higher order diffraction versus angle from the back focal plane image. As conventional images can be easily collected on the same microscope, the method provides a powerful tool for combining imaging metrology with scatterometry for optical critical dimension measurements in semiconductors.

Keywords: back focal plane, conoscopy, microscopy, optical critical dimension metrology, scatterometry, semiconductors

1. INTRODUCTION

As critical dimension (CD) measurements progress through the 45 nm node and beyond, there is increased urgency to develop techniques that can extend optical microscopy beyond the conventional diffraction limit. While gains can be made through traditional techniques such as reduction of the illumination wavelength and the use of immersion optics, another optical technique, scatterometry, routinely makes measurements on structures smaller than the diffraction limit. In scatterfield microscopy, we seek to realize nanometer-scale resolution in microscope-based tools, combining aspects of scatterometry, high-resolution microscopy, illumination engineering, and target design.[1,2]

It is well known that the back focal plane (BFP) of a bright-field reflection microscope contains diffraction information about the sample, as positions in the back focal plane map to diffraction angles from the sample.[3] With suitable control of the angle of the incident illumination, back focal plane imaging can provide information similar to that obtained from angle-resolved scatterometry.[4] In addition, while traditional scatterometry techniques typically measure scatter in a single plane of incidence, the back focal plane includes scatter out of the plane as well. This feature raises the potential for simultaneous imaging of multiple diffraction orders, investigation of diffraction from two-dimensional arrays, or observation of line edge or line width roughness in a manner similar to that recently demonstrated by Boher, *et al*., using optical Fourier transform scatterometry.[5] As with conventional scatterometry, the target need not be resolved in order for information to be obtained about it. Variations in line width, for example, on a grating target with pitch smaller than the diffraction limit will provide measurable changes in the zero-order diffraction which can be measured at the back focal plane, even though lines on such a target will be unresolved by conventional imaging using the same microscope.

*Correspondence: heather.patrick@nist.gov

In the present work, we demonstrate that combining back focal plane imaging with selected illumination angles yields an angle-resolved measurement of zero-order or multiple-order diffraction from a grating target in a single image. We have measured the zero-order reflectance signatures of grating scatterometry targets with pitches of 300 nm and 600 nm and line widths from 146 nm to 158 nm, and demonstrate nanometer-level sensitivity to line width with excellent repeatability. The necessary modifications to the microscope are easily implemented and provide a powerful tool that combines imaging metrology with scatterometry for optical critical dimension measurements.

2. PRINCIPLE OF OPERATION

2.1. Microscope configuration

Figure 1 shows the configuration of the microscope used in this work. The illuminator is a fiber-coupled Hg lamp. The end of this approximately 1 mm diameter fiber is imaged to a conjugate back focal plane, and the light passes through a linear polarizer and filter with a center wavelength of 546 nm. An amplitude mask is placed at the conjugate back focal plane, and its image is relayed to the back focal plane of a 100×, 0.95 numerical aperture (NA) microscope objective. Because position at the back focal plane maps to illumination angles at the sample,[3] the illumination mask serves to select the illumination angles incident upon the sample. The light that is diffracted by the sample at angles within the NA of the objective is collected, and a conoscopic (diffraction plane) image of the sample appears at the back focal plane of the objective. The image of the back focal plane of the objective was relayed to a 12-bit Dalsa Pantera[6] 1M60 charge-coupled device (CCD) camera using a Bertrand objective. An additional beamsplitter, which is not shown in Fig. 1, allowed conventional images of the sample to be collected at the same time.

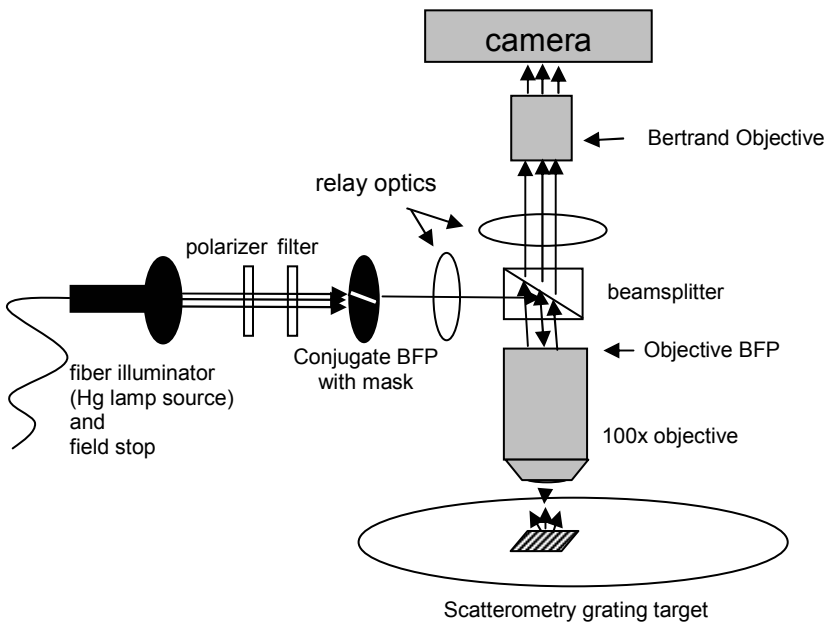

FIG. 1. Schematic of the microscope.

2.2. Selection and orientation of illumination mask

Figure 2 shows an overhead view of the orientation of two illumination masks with respect to the sample. For ease of viewing, the transmissive part of the mask is shown in black. In Fig. 2(a), a simple aperture is shown. If the aperture is small relative to the full back focal plane (shown as the large outer circle), this will select a specific incident angle. In

the case of Fig. 2(a), a non-zero angle of incidence, θ, is shown, with the plane of incidence perpendicular to the grating rulings. For a target with multiple diffraction orders for this angle and wavelength, an image of the diffraction pattern from the grating appears at the back focal plane, with the position of each order related to its diffraction angle θ by:

$$x = A \sin \theta \,, \tag{1}$$

where A is a constant that depends on the magnification of the objective and relay optics to the camera.

For the mask shown in Fig. 2(a), collecting diffracted intensity versus θ requires scanning the aperture in the back focal plane and collecting an image for each θ. Scanning was not required in the present work. Rather, a mask with a narrow slit as shown in Fig. 2(b) was used. In the case of a zero-order target, that is, a grating with only $m = 0$ diffraction for the range of incident angles and the wavelength used, the slit geometry allows a collection of the $m = 0$ diffracted intensity versus incident angle in a single image.

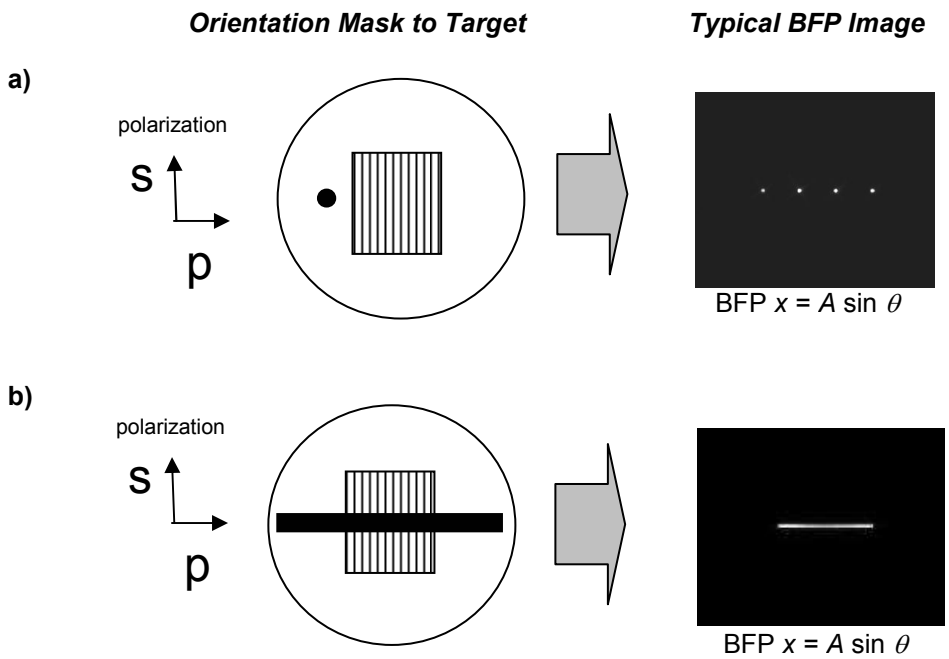

FIG. 2. Examples of illumination masks, and the corresponding image that is acquired by the camera. In (a), a single aperture selects a non-zero angle of incidence on a grating target of 1 μm pitch. The $m = -2, -1, 0$, and 1 diffraction orders are seen at the back focal plane. In (b), a long slit, perpendicular to the grating ruling, is shown. This slit selects a range of illumination angles, and the image at the back focal plane corresponds to the diffracted intensity at each collection angle. For a multi-order target, as in (a), this would result in overlapping diffraction orders. For the target shown in (b), the pitch is 300 nm, and only a single $m = 0$ order is collected over the range of incident angles available. This enables the collection of $m = 0$ diffracted intensity versus angle in a single image.

For targets with multiple diffracted orders, orienting the slit perpendicular to the target lines results in overlapping diffracted orders at the back focal plane. In this case, the slit can be angled slightly off the normal to the lines, such that the higher orders are separated from the $m = 0$ order, as shown in Fig. 3.

In addition to the angular selection made by the illumination mask, the polarization of the incident light was also controlled. For all targets, images were collected both with the electric field vector perpendicular to the plane of incidence (s-polarization) and with the electric field vector in the plane of incidence (p-polarization). An exception to this was made when the slit was angled for examining higher-order targets; the polarization was selected to be along the grating lines ("s") or perpendicular to the grating lines ("p"), although the plane of incidence was rotated slightly from the grating lines.

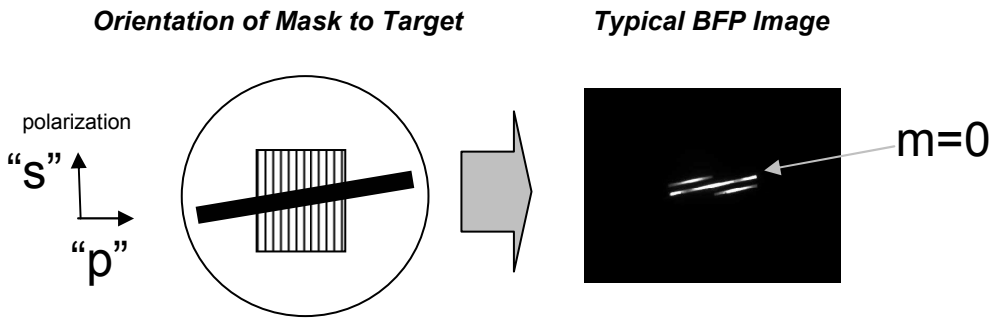

FIG. 3. Orientation of the slit with respect to the target used when the target pitch causes multiple diffraction orders to be present. A slight rotation of the slit with respect to the lines causes the $m = 0$ order to be separated from higher orders at the back focal plane. The slit angle was roughly 11°. Polarizations were defined with respect to the lines; although technically not true s- or p-polarization, they are referred to as "s" and "p".

3. DATA COLLECTION AND ANALYSIS

3.1. Target specifications and collection of back focal plane images

Back focal plane images were obtained from 100 µm × 100 µm scatterometry targets. The targets were produced using the SEMATECH Optical Metrology Advisory Group 3 (OMAG3) reticle.[7] The targets were etched silicon line gratings on a silicon substrate, with the line heights measured to be 228 nm using atomic force microscopy (AFM). The wafer was produced using a focus exposure matrix, such that targets on adjacent dies had fixed pitch, but different line widths. Two series of targets were investigated: zero-order targets of 300 nm pitch, and 600 nm pitch targets for which multiple diffraction orders were present.

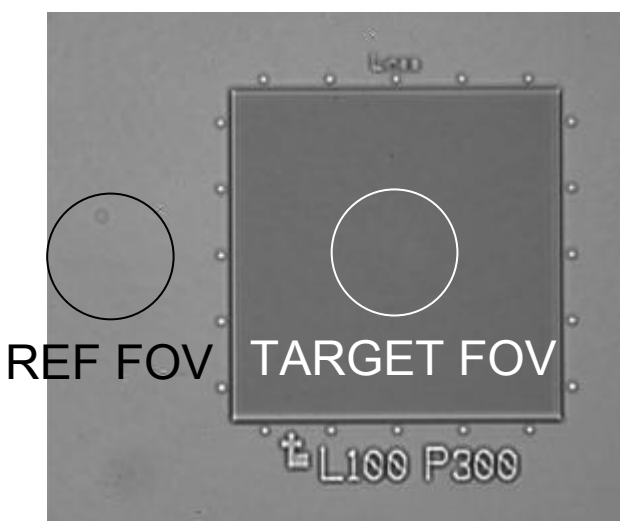

FIG. 4. Field of view (FOV) used for taking back focal plane images of the target and the flat silicon reference. The image shown was obtained using a 10× objective, while a 100× objective was used for actual data collection. The lines of the target, which are not resolved in this image, run vertically. The illumination slit orientation was horizontal relative to the target. The target was 100 µm on a side.

For a typical data run, back focal plane images were taken for targets of fixed pitch with varying line width. At each location on the wafer, two images were taken for the two linear polarizations. The approximate locations of the images

are shown in Fig. 4. The first image was a target image. The target was brought into approximate focus below the objective, with the microscope field stop reduced so that the illumination spot was approximately 30 µm in diameter. The second image was taken on a flat area of silicon adjacent to the target and was considered to be a reference image. In addition, a dark current image was taken for each data series, with no light reaching the camera.

3.2. Conversion of raw data to reflectance vs. angle

A raw back focal plane image appeared as a horizontal line, as shown in Fig. 2(b). After subtracting the dark current image, the target and reference images were converted to intensity in digital numbers (DN) from the camera CCD versus angle. The conversion factor A from back focal plane x-direction to θ in Eq. (1) was calibrated by fitting back focal plane images of the diffraction peaks from 2.75 µm and 1.98 µm pitch targets illuminated at 0°. The illumination angular range was approximately –60° to +60°, and was limited by the size of the image of the illuminating fiber end at the conjugate back focal plane. The polarization extinction of the light from the objective was verified to be better than 30:1. Data were averaged across the image height (the vertical direction shown in Fig. 2).

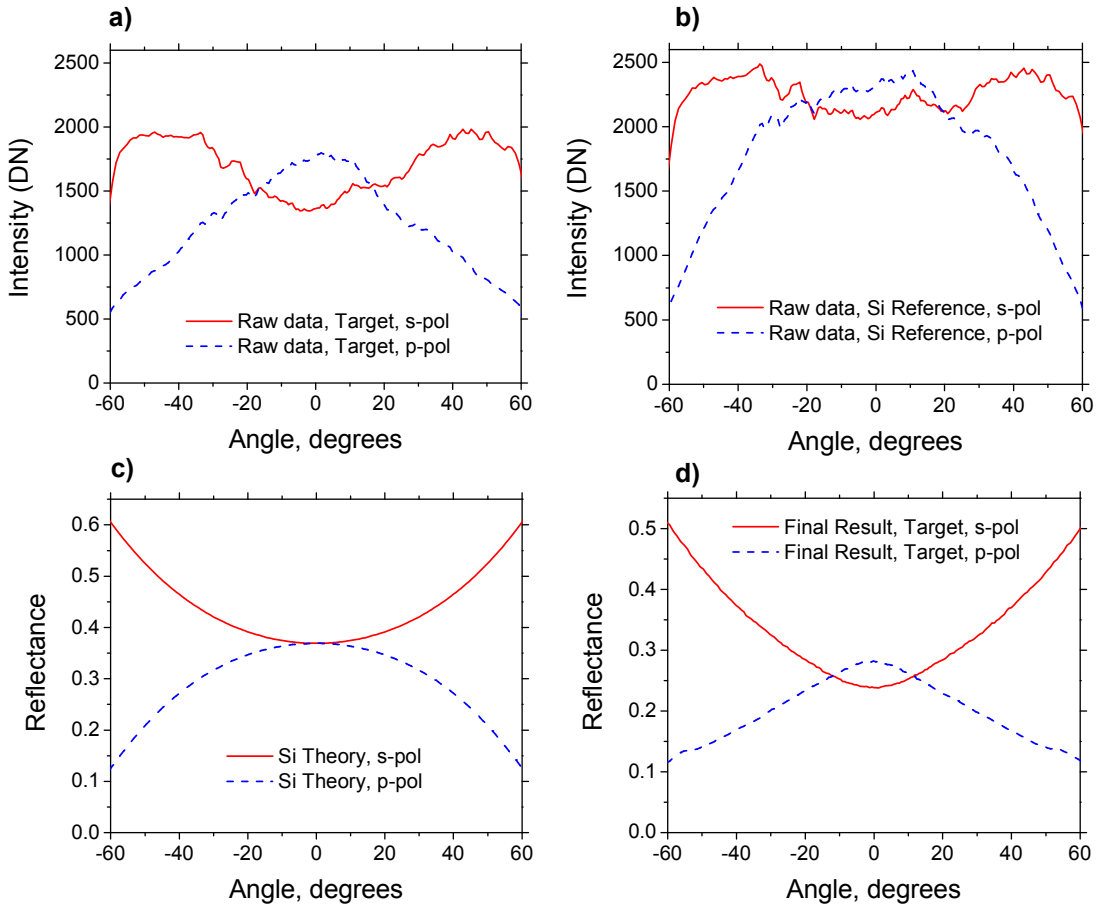

FIG. 5. Data analysis using silicon reference image and calculated silicon reflectance curve as discussed in the text. Graph (a) shows the raw data for (solid) s-polarization and for (dashed) p-polarization, taken from the target BFP image and reduced to intensity versus angle. The raw data is corrected using a reference BFP image (b) taken from a flat silicon area next to the target, and the calculated reflectance (c) of silicon versus angle. The final results for reflectance versus angle (d) for the target are obtained for each polarization by dividing the data in (a) by that in (b), and then multiplying by the data in (c).

The intensity versus angle data from typical target and reference images measured for s-polarization and p-polarization for a 300 nm pitch target are shown in Figs. 5(a) and 5(b). Although the data could be analyzed by comparing raw data, such as that shown in Fig. 5(a), from different targets, it is desirable to convert the intensity received at the camera to a true target reflectance value. However, there are angle- and polarization-dependent variations in transmission through the illumination and collection optics, as well as uncorrected variations in the source intensity versus angle, such that the conversion from raw data to reflectance is polarization and angle dependent. Fortunately, the apparent noise in the data shown in Figs. 5(a) and 5(b) was highly repeatable. Since bare silicon exhibits a well-known reflectance versus angle and polarization that can be calculated from its optical constants, we used the bare silicon reference image for each target to correct for the effects of source inhomogeneity and polarization-dependent transmission. The calculated reflectance versus angle for silicon is shown in Fig. 5(c). To convert raw target data shown in Fig. 5(a) to the target reflectance versus angle shown in Fig. 5(d), we divide the data in Fig. 5(a) by that in Fig. 5(b) and multiply the result by that in Fig. 5(c).

4. RESULTS AND DISCUSSION

4.1. Zero-order, 300 nm pitch targets

For the 300 nm pitch targets, nine targets were imaged, with multiple data collection runs on multiple days. Reflectance versus angle curves for three of the targets are shown in Fig. 6, with the s-polarization curves given in Fig. 6(a) and the p-polarization curves in Fig. 6(b). In the figure legend, the targets are identified by their die locations. The s- and p-curves for each target were highly repeatable. As in traditional scatterometry measurements, the exact shape of the curves is expected to be highly nonlinear and parameter dependent, requiring extensive library generation and comparison before the data could be used to obtain the target parameters. However, for the targets used in this investigation, the principal variable from target to target was line width; pitch, height, and optical constants were expected to remain fixed. For this reason, we give the line width (LW) in nanometers measured by scanning electron microscopy (SEM) for each target. Preliminary AFM measurements indicate there may also be small variations in sidewall angle from target to target.

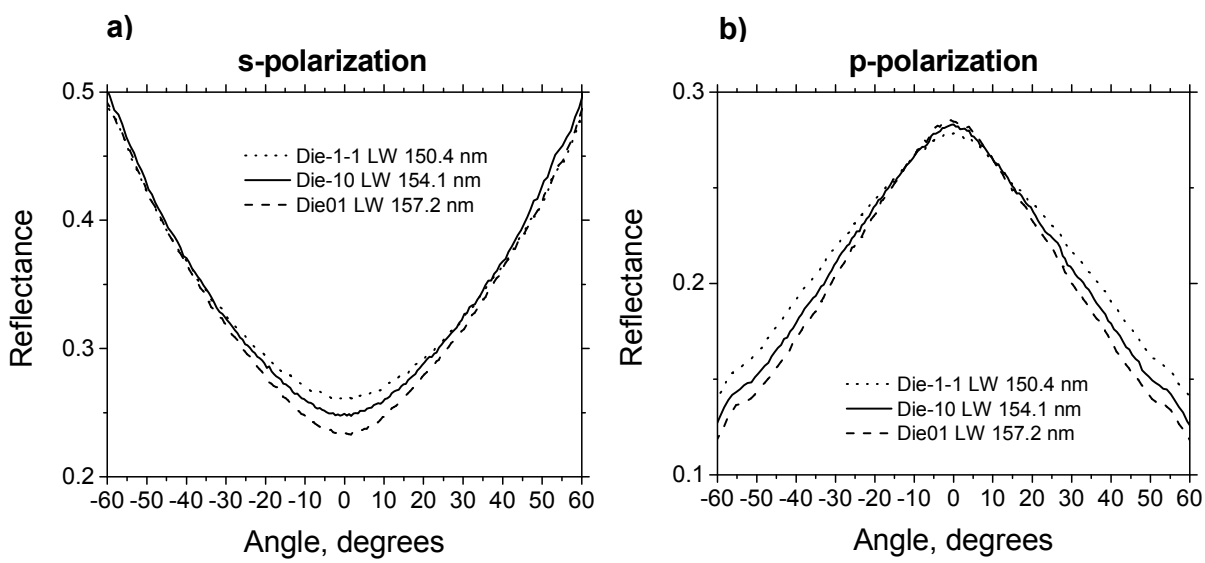

FIG. 6. Typical measured reflectance versus angle curves at s- and p-polarization for three 300 nm pitch targets of varying line width.

Figure 7 shows the repeatability and sensitivity of the measurements for s-polarization and p-polarization. We have plotted the reflectance obtained at 0° for s-polarization and –40° for p-polarization, for all of the measurements made on

all of the targets investigated. The reflectance is plotted versus the target line width as measured by SEM. Each target is represented by an individual symbol on the graph, with multiple occurrences of the symbol indicating the results of multiple optical measurements of that target taken on different days.

The x-error bars shown in Fig. 7 represent a single standard deviation of 27 SEM measurements of bottom line width made on each target. To estimate the y-error, we measured the repeatability of the intensity obtained at a fixed angle and sample by analyzing 10 consecutive silicon reference images taken using s- and p-polarization, then deriving the standard deviation of the intensity. The standard deviation of the intensity at 0° for s-polarization was 0.6 % and for p-polarization at –40° was 0.5 %. As each target measurement is normalized to a reference measurement when calculating reflectance, and because we expect similar repeatability in target and reference intensity, the percentage error for reflectance can be approximated by multiplying the above standard deviation by a factor of $\sqrt{2}$. The error bars shown in Fig. 7 are this percentage error multiplied by the measured reflectance. For many of the targets, the actual reflectances obtained from multiple measurements fall within the range of these y-error bars, as expected for a single standard deviation error estimate. Additional sources of error that could contribute to measurements falling outside this range include both lamp flicker between the acquisition of the reference and target image and variations in the exact location imaged on the target. Previous back focal plane scatterometry measurements indicated that exact focus position of the target did not yield a noticeable effect on results; however, this assumption may need to be revisited in future work. Accuracy of the measurements is discussed in Section 4.3.

The variation of reflectance at 0° (for s-polarization) and –40° (for p-polarization) with target line width can be used to quantify the sensitivity of the technique. As noted above, the expected behavior of reflectance versus angle for targets of different line width is highly parameter dependent, and the roughly linear dependence obtained at these angles and line widths would not be expected for all line widths. The results indicate nanometer-level sensitivity of the technique for the targets investigated. Given that dedicated angle-resolved scatterometry instruments routinely achieve sensitivity to line width in the sub-nanometer range,[8] it is reasonable that with proper control over the light source and a well-characterized transfer function through the optics, the current technique could be applied to a wide range of targets with good sensitivity.

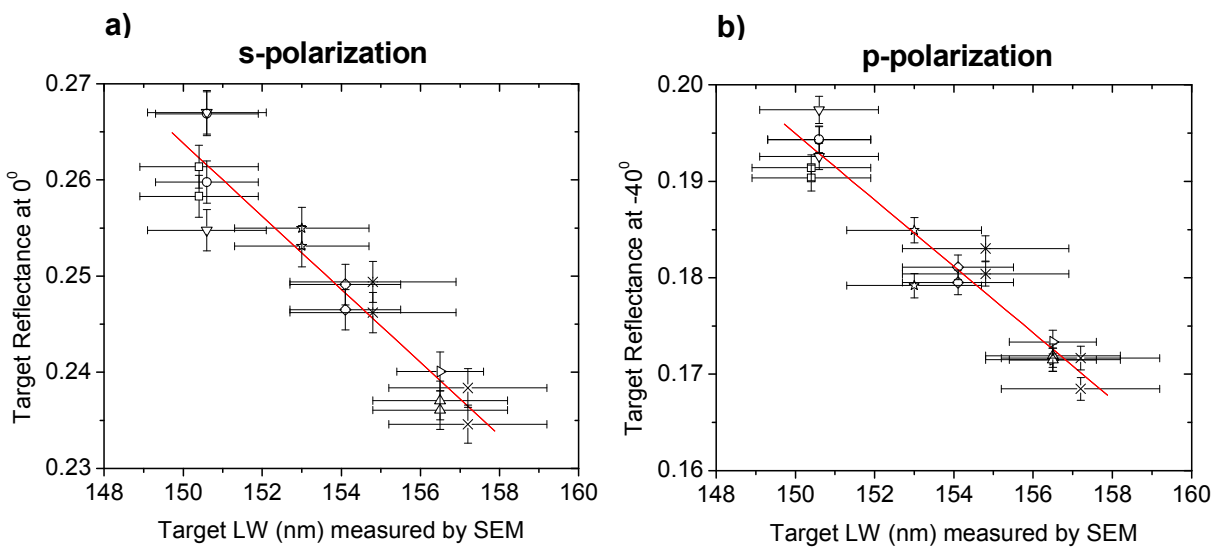

FIG. 7. System repeatability and sensitivity, as measured by the reflectance at (a) 0° for s-polarization and (b) –40° for p-polarization, for nine separate 300 nm pitch targets, versus target line width as measured by SEM. Each symbol represents a single target, with multiple occurrences of that symbol indicating multiple optical measurements of the target.

4.2. 600 nm pitch target series with multiple diffraction orders

We also investigated a series of 600 nm pitch targets with varying line width. For this series, the slit was angled relative to the target lines as shown in Fig. 3. Typical results for the $m = 0$ reflectance are shown in Fig. 8. Four targets are shown for the "s" and "p" polarization cases.

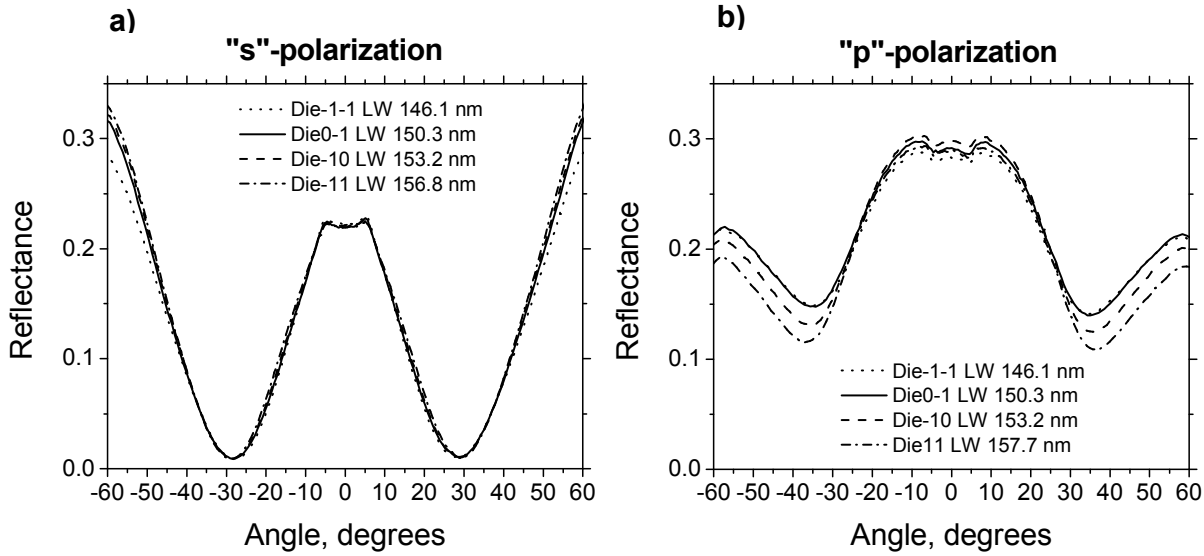

FIG. 8. Typical measured reflectance versus angle curves for "s"- and "p"-polarization for 600 nm pitch targets of varying line widths.

As with the 300 nm pitch targets, the reflectance curves show line width sensitivity. For this target, the "p" polarization gave better sensitivity, except at the smallest line width, 146.1 nm. We believe this to be a real effect – it is quite possible that the "p"-polarization sensitivity is at an inflection point here, and there is sensitivity shown in "s" polarization at this line width. The repeatability was not separately investigated for these targets, but is expected to be similar to that obtained for the 300 nm pitch targets. Our ability to separate the diffraction orders by angling the slit gives the possibility of collecting and analyzing multiple order diffraction peaks at once.

4.3. Accuracy and System Limitations

Discussion of the above results for both the 300 nm pitch and the 600 nm pitch targets would not be complete without considering the accuracy and dynamic range of the system for obtaining reflectance versus angle. In the current implementation, the requirement for a reference image and the calibration of the target image reflectance from the reference, while giving good repeatability and sensitivity, has the potential to introduce errors in accuracy, particularly at large incident angles for p-polarization. The final value for target reflectance at a given angle depends on the determination of the constant A in Eq. (1), not only as a scaling from x to θ, but also because the values of the theoretical silicon reflectance curve are calculated using θ. The nonlinear relationship between A and θ makes the effect larger at high angles of incidence. For example, a 1 % change in A at a value of x that corresponds to $\theta = 10°$ changes the calculated θ by only 0.1°, but at a value of x that corresponds to $\theta = 60°$ changes θ by 1°. This effect is compounded by the nonlinear change in silicon reflectance versus angle, which also has a steeper slope at higher angles (over the range used here). At $\theta = 10°$, a $\Delta\theta = 0.1°$ only changes R_p and R_s of silicon by ~0.0001 (out of $R_s = 0.37$ or $R_p = 0.36$), while at $\theta = 60°$, a $\Delta\theta = 1°$ changes R_p and R_s of silicon by ~0.009 (out of $R_s = 0.61$ or $R_p = 0.12$). Since the target data is multiplied by the silicon R_s or R_p, this leads to a worst-case change in the calculated target reflectance corresponding to a given value of BFP x of 7.5 %, for p-polarization at $\theta = 60°$. This accuracy can of course be improved by limiting the data collection to lower incident angles. It should be stressed that this does not change the sensitivity of the system, as once a value for A

has been chosen all reflectance curves are calibrated with the same theoretical reflectance values, but rather the accuracy of the reflectance measured at a given angle. This effect should be carefully considered when designing such a system for accurate reflectance measurements and when comparing these measurements to theory and to other scatterometry methods.

Polarization also plays an important role in the accuracy of the target reflectance measurements. The polarization extinction of the light from the objective was verified to be better than 30:1 for the incident angles used; however, polarization was not controlled on the collection side of the optics and may need to be considered when comparing these results to those from other scatterometry techniques. It can also be seen from comparing Fig. 2(b) (the experimentally measured reflectance versus angle from the flat silicon surface) with Fig. 2(c) (the theoretical reflectance of silicon versus angle) that there is significant polarization-dependent transmission through the optics, particularly for s-polarization. This is not surprising, given that s-polarization generally is not transmitted as well as p-polarization through optics at high angles of incidence. Although we plan to continue to characterize and hopefully reduce the sources of this polarization dependence, it is unlikely that it can be eliminated from the system. We also plan to explore the possibilities for performing ellipsometric measurements with this or a similar instrument.[9]

Additional limitations of the current system include dynamic range and the requirement for dark current subtraction. The targets investigated in this work had a small dynamic range of reflectance, such that the camera could be operated with signal levels that were typically 2 to 3 orders of magnitude greater than the dark current. However, for targets with larger variations in reflectance, dark current subtraction could become problematic and a cooled detector may be required. Dynamic range may be improved by using a 16-bit camera. Camera linearity is of course also extremely important for this measurement. Though the current camera was verified to give a linear response of DN values versus light intensity, the camera linearity must be well known before the system accuracy can be fully characterized.

5. FUTURE WORK

In the present study, we have shown that back focal plane imaging combined with suitable control of the incident angles can provide sensitive, repeatable measurements of angle-resolved reflectance on zero-order and higher-order grating scatterometry targets. This work demonstrates the feasibility of combining scatterometry and imaging metrology in a standard optical microscope, and lays the groundwork for the application of this aspect of scatterfield microscopy to optical critical dimension metrology. Future areas of investigation may include

- Improvements in illumination uniformity and enhancements to amplitude and polarization control
- Investigation of out-of-plane scatterometry from 2-D targets
- Accuracy of the system
- Comparison of results to other scatterometry instruments and to theoretical calculations
- Limitations to reduction of target size

ACKNOWLEDGEMENTS

The authors would like to thank International SEMATECH for metrology and wafer fabrication support and Ron Dixson of NIST for AFM measurements.

REFERENCES

1. R.M. Silver, R. Attota, M. Stocker, M. Bishop, L. Howard, T. Germer, E. Mar, M. Davidson and R. Larrabee, "High-resolution optical metrology," in *Metrology, Inspection, and Process control for Microlithography XIX*, R.M.Silver, Ed., Proc. SPIE **5752**, 67-79, (2005).
2. R. Attota, R.M. Silver, T.A. Germer, M. Bishop, R. Larrabee, M.T. Stocker and L. Howard, "Application of through-focus focus-metric analysis in high resolution optical metrology," in *Metrology, Inspection, and Process control for Microlithography XIX*, R.M.Silver, Ed., Proc. SPIE **5752**, 1441-1449, (2005).
3. S. Inoue and R. Oldenbourg, "Microscopes", in M. Bass, E.W. Van Stryland, D.R. Williams and W.L.Wolfe (eds.), *Handbook of Optics, Volume II*, 2d ed., McGraw-Hill, New York, 1995, pp. 17.39-17.40.

4. C.J. Raymond, M. R. Murnane, S. Naqvi, and J.R. McNeil, "Metrology of subwavelength photoresist gratings using optical scatterometry ," J. Vac. Sci. Technol. B **13(4)**, 1484-1495 (1995).
5. P.Boher, J. Petit, T. Leroux, J. Foucher, Y. Desieres, J. Hazart and P. Chaton,, "Optical Fourier transform scatterometry for LER and LWR metrology," in *Metrology, Inspection, and Process control for Microlithography XIX*, R.M.Silver, Ed., Proc. SPIE **5752**, 192-203, (2005).
6. We use the trade name to specify the experimental procedure adequately and do not imply endorsement by the National Institute of Standards and Technology.
7. B. Bunday, M. Bishop, and R. Silver, "The OMAG3 Reticle Set," SEMATECH Document ID# 03074417A, available at www.sematech.org, (2003).
8. Yi-sha Ku, Ding-Sheng Pan, Shih-Chun Wang, C.H. Tung, Chun-Hung Ko, and Sheng-Hua Lu, "Performance study of CD mark size for angular scatterometry," in *Metrology, Inspection, and Process control for Microlithography XIX*, R.M.Silver, Ed., Proc. SPIE **5752**, 59-66, (2005).
9 Qiwen Zhan and James R. Leger, "Measurement of surface features beyond the diffraction limit with an imaging ellipsometer," Opt. Lett. **27**, 821-823 (2002).